ACS APPLIED MATERIALS & INTERFACES

Research Article

www.acsami.org

Organic Bulk Heterojunction Photovoltaic Devices Based on Polythiophene–Graphene Composites

Minas M. Stylianakis,[†,‡] Emmanuel Stratakis,[†,§,⊥] Emmanuel Koudoumas,[†] Emmanuel Kymakis,*[,†] and Spiros H. Anastasiadis[‡,§]

[†] Center of Materials Technology and Photonics & Electrical Engineering Department, Technological Educational Institute (TEI) of Crete, Heraklion 71004 Crete, Greece

[‡] Department of Chemistry, University of Crete, P.O. Box 2208, 710 03 Heraklion Crete, Greece

[§] Institute of Electronic Structure and Laser, Foundation for Research and Technology–Hellas, P.O. Box 1527, 711 10 Heraklion Crete, Greece

[⊥] Department of Materials Science and Technology, University of Crete, Heraklion, 71003 Crete, Greece

ABSTRACT: A solution-processed graphene content was synthesized by treatment of graphite oxide (GO) with phenyl isothiocyanate (PITC) by taking advantage of the functional carboxyl groups of graphene oxide. The GO was prepared by the oxidation of natural graphite powder and was expanded by ultrasonication in order to exfoliate single or/and few-layered graphene oxide sheets. The functionalized graphene oxide, GO-PITC, can be dispersed within poly-(3-hexylthiophene) (P3HT) and can be utilized as the electron acceptor in bulk heterojunction polymer photovoltaic cells. When P3HT is doped with GO-PITC, a great quenching of the photoluminescence of the P3HT occurred, indicating a strong electron transfer from the P3HT to the GO-PITC. The utilization of GO-PITC as the electron acceptor material in poly-(3-hexylthiophene) (P3HT) bulk heterojunction photovoltaic devices was demonstrated, yielding in a power conversion efficiency enhancement of 2 orders of magnitude compared with that of pristine P3HT.

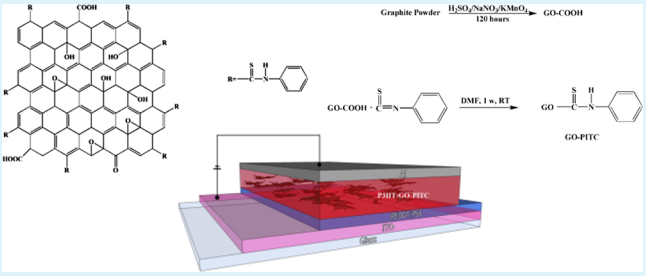

KEYWORDS: *graphene, photovoltaic, functionalization, solution-processed, bulk heterojunction*

1. INTRODUCTION

Novel carbon-based structures, such as carbon nanotubes and graphene, have emerged in recent years as integrative materials for organic photovoltaic devices.[1−9] The most recent building block of intriguing actual scientific and technological interest is graphene, best described as a two-dimensional (2D) single-atom-thick sheet of sp^2-hybridized carbon atoms arranged in a honeycomb lattice with outstanding electronic, mechanical, thermal, and chemical properties.[10,11] However, the liquid-phase production of graphene-based materials is severely hampered by the low yield of graphene exfoliation (a few graphene monolayers per square millimeter of substrate area) and its poor solubility in common organic solvents,[12] which is mainly due to the attractive van der Waals forces between the graphene sheets.[13,14] So far, the response to the problem of low yield has been the exfoliation of chemically modified forms of graphene, such as graphene oxide (GO), or functionalized graphene,[15−17] or the exfoliation of graphene from graphite under intense sonication in water or organic solvents.[18] On the other hand, graphene sheets are functionalized by covalent or noncovalent coupling modifications in order to increase their solubility in organic solvents or within a polymer matrix.[19−21] The advantage of using noncovalent functionalization via $\pi-\pi^*$ stacking and hydrophobic interactions instead of covalent functionalization is that the intrinsic properties of graphene are preserved.[22−25] Furthermore, since the pristine graphene is zero bandgap, the introduction of the functional groups opens up the bandgap of the functionalized graphene. Therefore, graphene-based materials are anticipated to be utilized for the effective exciton separation and charge transport when blended with conjugated polymers, because of the large surface area for donor/acceptor interfaces and continuous pathway for the electron transfer, as in the case of carbon nanotubes.[26−30] Chemical routes, such as those based on Hummers' oxidation method, have been explored as means to introduce a large number of abundant functional groups within the graphene structure, such as hydroxyl (−OH), aldehyde (−CHO), carboxyl (−COOH) or epoxyl ones, thus reducing the interplane forces and imparting hydrophilic character.[31] Moreover, many different functional moieties (amino, bromine, long alkyl chain, etc.) as well as polymer chains (e.g., poly(ethylene glycol), polystyrene) have been anchored onto the graphene oxide sheets by various chemical approaches.[32]

Received: July 2, 2012
Accepted: August 16, 2012
Published: August 16, 2012

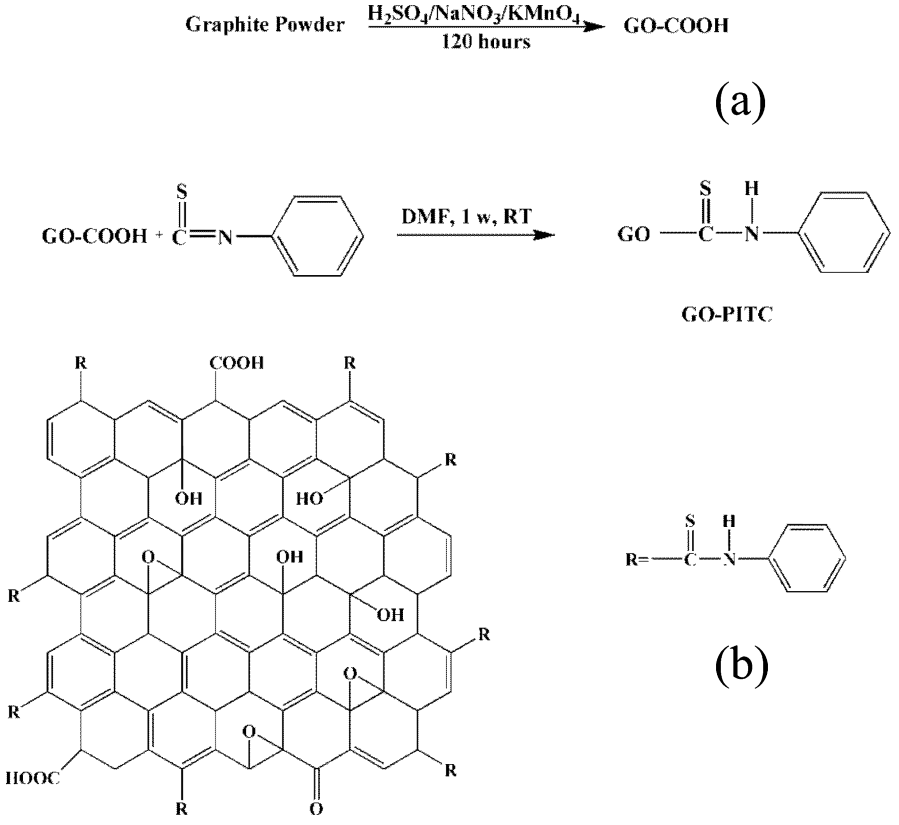

Figure 1. Schematic representation of (a) the chemical synthesis and (b) the structure of the solution-processed GO-PITC by functionalization of GO.

In this paper, a facile method is described that allows the chemical treatment of GO sheets with phenyl isothiocyanate (PITC). This results in a solution processable graphene based material, namely GO-PITC, which can be integrated in organic photovoltaic devices, due to its unique structural and photophysical properties. GO-PITC displays increased solubility in common organic solvents as compared to that of the untreated GO. The synthesized GO-PITC is blended with the conjugated polymer poly(3-hexylthiophene), P3HT, in different concentrations. The structure and morphology of the polythiophene-graphene composites are characterized by X-ray diffraction (XRD) and field-emission scanning electron microscopy (FE-SEM), whereas their spectroscopic properties are investigated by fluorescence, UV/vis and Raman spectroscopies. It is demonstrated that the utilization of GO-PITC in photovoltaic devices with the structure glass/ITO/PEDOT:PSS/P3HT:GO-PITC/Al lead to devices that exhibit photovoltaic performance, significantly better (power conversion efficiency 2 orders of magnitude higher) than that of the pristine P3HT device, indicating the potential of utilizing GO-PITC as an electron acceptor material.

2. EXPERIMENTAL SECTION

2.1. Preparation of Graphene Oxide (GO). GO was prepared from purified natural graphite powder (Alfa Aesar, ~200 mesh) according to a modified Hummers' method[33] and purified by a controlled centrifugation method;[34] the procedure is schematically depicted in Figure 1a. Specifically, graphite powder (0.5 g) was placed into a cold mixture of concentrated H_2SO_4 (40 mL, 98%) and $NaNO_3$ (0.375 g) under vigorous stirring for 1 h, in an ice bath. During this time $KMnO_4$ (2.25 g) was added in small portions and the ice bath was kept for 2 h more, in order to cool the mixture below 10 °C. The green-brown colored mixture remained under stirring for five days. On completion of the reaction, the brick-colored mixture was mixed with an aqueous solution of 5% H_2SO_4 (70 mL). The mixture was stirred for one hour under heating at 98 °C and became gray-black colored. When the temperature decreased to 60 °C, 30% H_2O_2 (~2 mL) was added and the mixture was stirred for 2 h at room temperature. The mixture was, then, centrifuged for 5 min at 4200 rpm and washed with ~600 mL of an aqueous solution of 3% H_2SO_4 (~9 mL)/0.5% H_2O_2 (~1.5 mL) in order to remove the acidic anions, especially these of Mn. Then, it was put in an ultrasonic vibration bath for 10 min so that the ultrasonic vibration would exfoliate the graphite oxide to GO sheets. The process was repeated 10 times. Then, the mixture was washed and purified with 150 mL of aqueous solution 3% HCl (~1.5 mL) for 3 times. Afterward, it was washed thoroughly with deionized water (DI) and acetone, in order to remove any acidic part remaining. Finally, the resulting GO was dried at 60 °C under vacuum oven overnight.

2.2. Preparation of GO-PITC. GO (200 mg) was placed in a flask with 20 mL of anhydrous dimethylformamide, DMF. The mixture was ultrasonicated for 20 min to give a homogeneous suspension. An amount (20 g) of phenyl isothiocyanate, PITC, was then added to the mixture. The mixture was stirred for one week at room temperature, under nitrogen. The functionalized GO, GO-PITC, was purified and isolated by repeating the procedure below three times, thus, by taking advantage of its hydrophobic nature, in contrast to the hydrophilic GO.[35] The suspension was added dropwise to 1,2-orthodichlorobenzene, o-DCB, (~30 mL),stirred and centrifuged at 800 rpm for 8 min. The supernatant solution was added dropwise to $CHCl_3$ (~50 mL), stirred and centrifuged at 4200 rpm for 20 min. The resulting GO-PITC was dried overnight in a vacuum oven (124 mg, yield 62%). The synthesis and the structure of GO-PITC are schematically depicted in the lower part of Figure 1a and in Figure 1b, respectively.

2.3. Fabrication and Characterization of Photovoltaic Devices. All the photovoltaic (PV) devices were fabricated in a sandwich geometry consisting of a bottom indium tin oxide (ITO)

dx.doi.org/10.1021/am301204g | ACS Appl. Mater. Interfaces 2012, 4, 4864−4870

coated electrode, a P3HT:GO-PITC thin film, and a top metal (Al) electrode. Indium tin oxide (ITO, 15 Ω/sq) coated glass substrates were used for the device fabrication. The substrates were cleaned by 10 min consecutive sonication in detergent, deionized water, acetone and isopropyl alcohol, in an ultrasonic bath (Elma S 30 H Elmasonic). Poly(3,4-ethylenedioxythiophene):poly(styrenesulfonate), PEDOT:PSS, (Clevios P Al 4083, ∼30 nm thickness) thin film was spin coated onto the clean substrates, which were subsequently dried at 120 °C for 10 min to remove any residual water. Photovoltaic devices were then fabricated, in air, by spin coating a P3HT:GO-PITC thin film (110 nm) from its *o*-DCB solution (concentration 17 mg/mL), followed by annealing at 160 °C for 20 min. Thereafter, an Al electrode (80 nm) was deposited by vacuum evaporation onto the active layer through a shadow mask to define an active area of 18 mm^2 for each device. Current−voltage ($J-V$) measurements were performed at room temperature using an Agilent B1500A Semiconductor Device Analyzer. For photovoltaic characterization the devices were illuminated with 100 mW/cm^2 power intensity of white light by an Oriel solar simulator with an AM1.5 filter through the glass/ITO side. All measurements were made in air immediately after device fabrication.

2.4. Microscopic and Spectroscopic Characterization. The samples were characterized by Raman spectroscopy at room temperature utilizing a Nicolet Almega XR Raman spectrometer (Thermo Scientific) with a 473 nm blue laser as an excitation source. Fourier transform infrared (FTIR) spectra were measured on a Bruker FTIR spectrometer IFS 66v/F (MIR). The photoluminescence (PL) measurements were carried out in the wavelength range from 500 to 1000 nm using a He−Cd cw laser (325 nm) with a full power of 35 mW as the excitation source. UV−vis absorption spectra were recorded using a Shimadzu UV-2401 PC spectrophotometer over the wavelength range of 300−800 nm. The morphology of the surfaces was examined by field emission scanning electron microscopy (FE-SEM JEOLJSM-7000F) and by atomic force microscopy (AFM-Digital Instruments NanoScope IIIa). X-ray diffraction patterns were collected on a Panalytical Expert Pro X-ray diffractometer, using Cu Kα radiation (λ = 1.5406 Å). Thermogravimetric analysis (TGA) was performed on 5−10 mg samples over the temperature range from 40 to 800 °C at a heating rate of 10 °C/min utilizing a Perkin-Elmer Diamond Pyris model under nitrogen atmosphere.

3. RESULTS AND DISCUSSION

The GO and GO-PITC powders are analyzed by means of FTIR spectroscopy and the results are shown in Figure 2. The O−H stretching vibration appears as a broad peak at 3390 cm^{-1}. The most characteristic features in the FTIR spectrum of GO are the adsorption bands corresponding to the C═O carbonyl stretching at 1670 wavenumbers (cm^{-1}), the C−OH stretching at 1220 cm^{-1}, and the C−O stretching at 1053 cm^{-1}. Similar to that of GO, the FTIR spectrum of GO-PITC exhibit the characteristic C═O stretching at 1652 cm^{-1} of the carbonyl groups. The band at ∼1600 cm^{-1} can be assigned to the amide carbonyl stretching mode. The new band at 1541 cm^{-1} can originate from either amides or carbamate esters and corresponds to the coupling of the C−N stretching vibration with the CHN deformation vibration.[36] Even more importantly, the FTIR spectrum of GO-PITC displays a characteristic peak at ∼2115 cm^{-1} associated with the isothiocyanate group, indicating that, indeed, the GO was successfully functionalized with phenyl isothiocyanate. In order to investigate the absorption behavior of GO and GO-PITC films, we have prepared thin films by spin-coating onto quartz substrates and the normalized UV−vis absorption spectra of pure GO and GO-PITC are shown in Figure 3. The absorption spectrum of GO-PITC (red line) is red-shifted compared to the pure GO (black line).

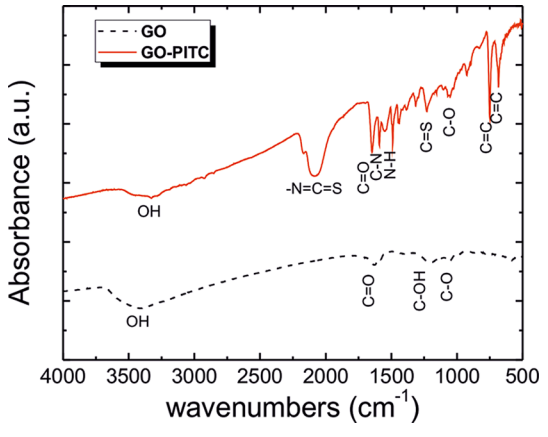

Figure 2. FTIR spectra of pure GO (black line) and GO-PITC (red line) in transmission mode.

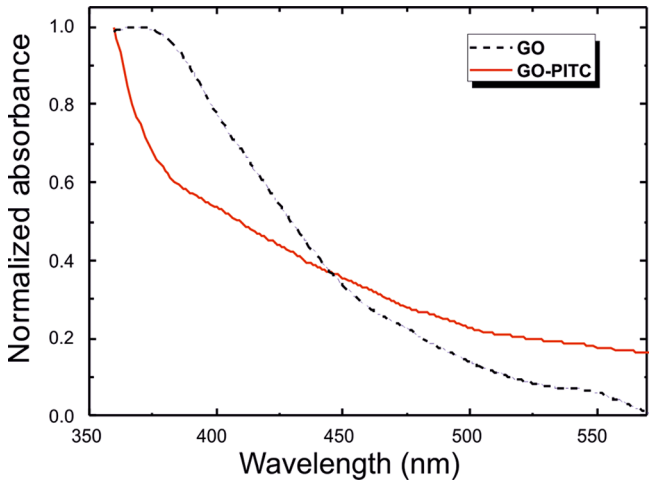

Figure 3. Normalized UV−vis absorption spectra of pure GO (black line) and GO-PITC (red line) in thin solid films prepared by spin-coating onto a quartz substrate.

Raman spectroscopy is the most direct and nondestructive technique to characterize the structure and quality of carbon-based materials, particularly in order to determine defects, ordered and disordered structures, and the layers of graphene. For the measurement, a laser excitation of 473 nm was used, and powder samples were directly deposited on a Si wafer without using any solvents. Figure 4 shows the Raman spectra of GO and GO-PITC powders, which exhibit two dominant peaks at around 1350 and 1580 cm^{-1} that correspond to the well-defined D and G bands, respectively. The Raman spectra reveal the dramatic changes in the signals of the GO-PITC upon functionalization. GO-PITC exhibits a higher D/G intensity ratio (I_D/I_G) relatively to GO; this attests to the successful functionalization of GO by the formation of covalent bonds between GO and PITC.[37] The Raman shift of the D and for GO-PITC (from 1342 to 1355 cm^{-1}) provides evidence for the charge transfer between the GO sheets and the PITC functional group.

The data from the thermogravimetric analysis (TGA), are presented in Figure 5. GO begins to lose mass upon heating even below 100 °C and has resulted in a rapid mass loss commencing at about 200 °C, probably due to pyrolysis of labile oxygen-containing functional groups, such as −OH, −CO

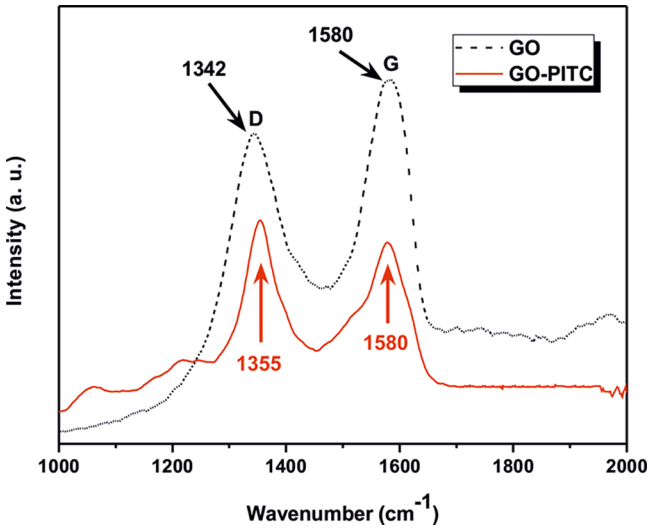

Figure 4. Raman spectra of GO (black line) and GO-PITC (red line), obtained utilizing an incident laser at 473 nm.

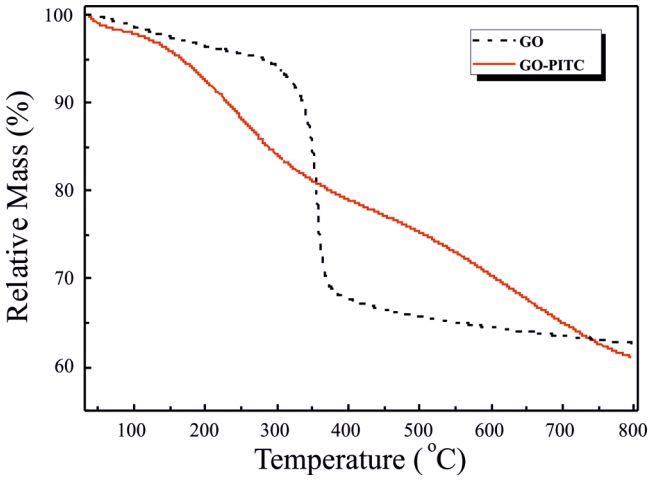

Figure 5. Thermogravimetric (TGA) data of GO (black line) and GO-PITC (red line) obtained under an inert nitrogen atmosphere with a heating rate of 10 °C/min.

and −COOH groups, and a total mass loss of ∼40% at 800 °C, in agreement with data in the literature.[38] In contrast, GO-PITC displays improved thermal stability until 700 °C. Briefly, the TGA curve of GO-PITC shows a 4% weight loss before 150 °C, due to the humidity and the evaporation of traces of remaining solvent. In the range of 150 to 370 °C, a weight loss of ca. 20% occurred due to the decomposition of oxygen-containing and isothiocyanate functional groups. From 370 to 800 °C, a weight loss of ∼40% was observed, which can be attributed to the removal of the phenyl side rings of the functionalized graphene oxide sheets. The TGA analysis further confirms that GO was successfully functionalized.

The as-prepared GO and GO-PITC samples were also characterized by X-ray diffraction (XRD), Figure 6. The diffraction peak at 2θ = 13.2° has been attributed to the (002) main reflection of stacks of graphene oxide with a 6.7 Å interlayer distance and a finite number of layers (∼18). The diffractogram of GO-PITC does not exhibit the peak at 13.2°; instead peak is observed at 9.5° together with a smaller one at 19.0°; the former should be attributed to the interplanar spacing of the disordered stacking of functionalized graphene

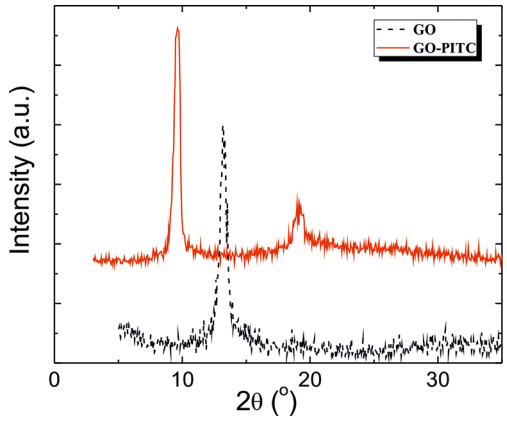

Figure 6. X-ray diffraction patterns of GO (black line) and GO-PITC (red line) powder samples.

oxide sheets,[39,40] i.e., of GO-PITC, with a 9.1 Å interplanar distance and ∼17 layers. The peak at 19.0° may be due to a partial reduction of GO during the functionalization reaction of GO to GO-PITC. In order to investigate the morphology of GO-PITC, scanning electron microscopy (SEM) and atomic force microscopy (AFM) were used and the images are shown in Figure 7. GO-PITC exhibits a wrinkled and crinkly structure, like plane tree leaves, with a smooth surface. One should note that the network of graphene-based sheets and the individual GO-PITC sheets are electrically conductive since no charging was observed during the SEM imaging. Furthermore, AFM analysis indicated significant exfoliation of the pristine graphene flakes, leading to sheet thicknesses in the 2−20 nm range

Figure 8 displays the normalized UV−vis absorption spectra of P3HT and of the P3HT:GO-PITC composite in thin films, prepared by spin-coating onto quartz substrates. The UV−vis spectrum of P3HT:GO-PITC composite is about 35 nm red-shifted compared with that of the pristine P3HT film. This shift is due to a sufficiently increased chain motion, indicating an increase in the crystalline ordering, resulting in a stabilization of the P3HT chains.[41] Also, the presence of GO-PITC in the active layer exhibits a better light-absorbing ability. Therefore, the relatively acceptor content (20%) at which the optimized power-conversion efficiency can be obtained, indicates the great superiority of the GO-PITC used as the electron acceptor material.

Figure 9 depicts the photoluminescence (PL) spectra of pure P3HT and of P3HT:GO-PITC (20%), in thin solid films, on Si substrates, at an excitation wavelength of 325 nm. The data for the film of pure P3HT shows a very strong emission band over the range 650−700 nm, which is apparently extinguished, due to the fluorescence-quenching effect due to the GO-PITC graphene content.[35] This phenomenon illustrates that GO-PITC can be used as a strong electron acceptor moiety in bulk heterojunction (BHJ) devices.

Figure 10 displays the surface morphology of the P3HT and the P3HT:GO-PITC (20 wt %). composite films by the use of AFM. The GO-PITC is well dispersed in the P3HT matrix, and no agglomerates formed by aggregates sheets are present. Furthermore, the surface of the composite is smoother than the pristine P3HT film, and a fine "packaging" of the two blend components can be observed.

Finally, bulk heterojunction photovoltaic devices were fabricated utilizing the GO-PITC as the electron acceptor, and the P3HT as the electron donor. Two different ratios of

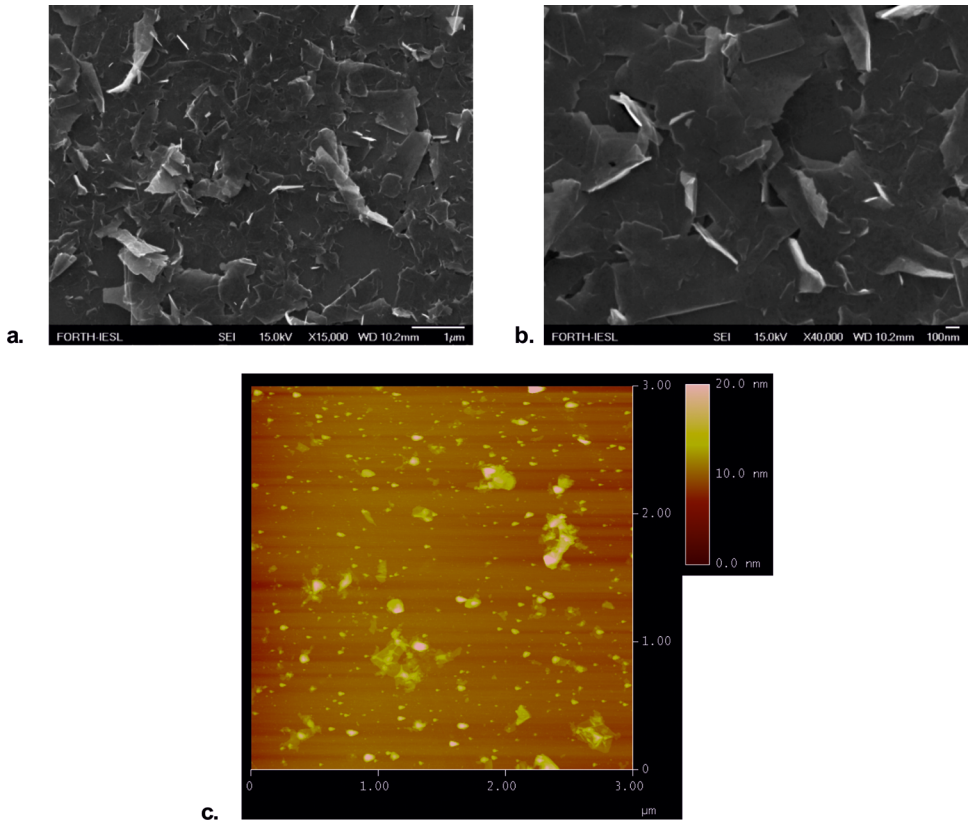

Figure 7. Field-emission scanning electron microscopy (FE-SEM) images of GO-PITC in (a) plane tree leaves, (b) wrapped graphene-based sheets, and (c) AFM image of GO-PITC.

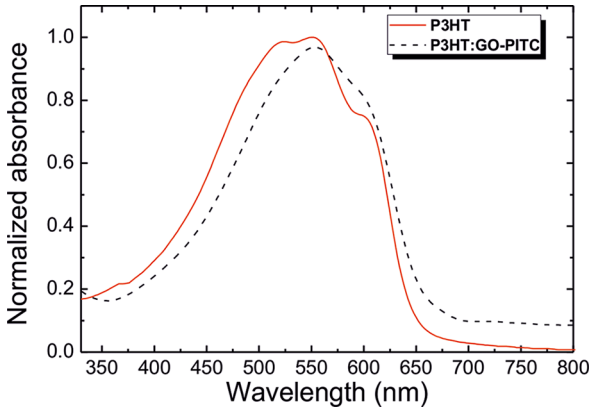

Figure 8. Normalized UV−vis absorption spectra of P3HT (red line) and of the P3HT:GO-PITC (black line) composite in thin films onto quartz substrates.

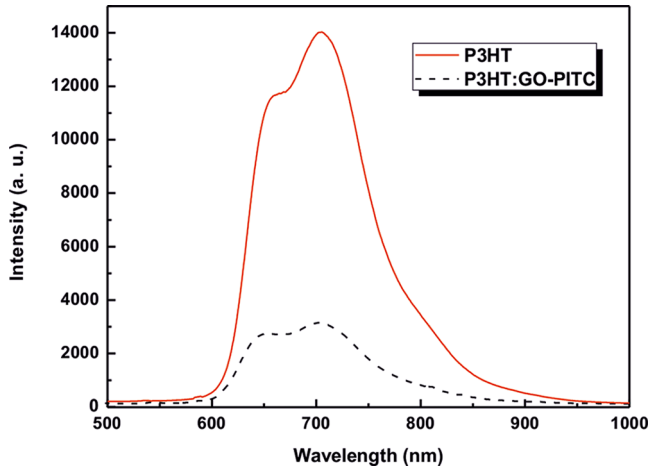

Figure 9. Photoluminescence (PL) spectra of P3HT (red line) and P3HT:GO-PITC 20% (black line) in thin film on a Si substrate at an excitation wavelength of 325 nm.

GO-PITC to P3HT were used (10 and 20 wt %). The structure of the device is, thus, ITO/PEDOT:PSS (30 nm)/P3HT:GO-PITC (110 nm)/Al (80 nm), schematically shown in Figure 11a. A postfabrication annealing of the P3HT:GO-PITC active layer, conducted at 160 °C for 20 min under N_2 atmosphere, improves the morphology of the film and removes residual functional groups linked to the graphene sheet. As a result, the conjugation length increases and the charge transport mobility is enhanced.[42] Figure 11b shows the current voltage (J−V) curves for the photovoltaic devices with GO-PITC content of 10 and 20 wt %. Table 1 displays the photovoltaic characteristics and points out that the device containing 20% GO-PITC shows a better photovoltaic performance exhibiting an open-circuit voltage (V_{oc}) of 0.51 V, short-circuit current density (J_{sc}) of 4.34 mA/cm^2, fill factor (FF) of 46%, and power conversion efficiency (η) of 1.02%, more than 2 orders of magnitude larger than the efficiency of the pristine P3HT device. Moreover, the device with 10% GO-PITC achieved power conversion efficiency (η) of 0.88% with a V_{oc} of 0.57 V, a J_{sc} of 3.96 mA/cm^2, and a FF of 39%. The efficiency increased when the concentration of the graphene content increased relatively to P3HT. When even higher concentrations of GO-PITC were used, large aggregates were formed, which hindered

dx.doi.org/10.1021/am301204g | ACS Appl. Mater. Interfaces 2012, 4, 4864−4870

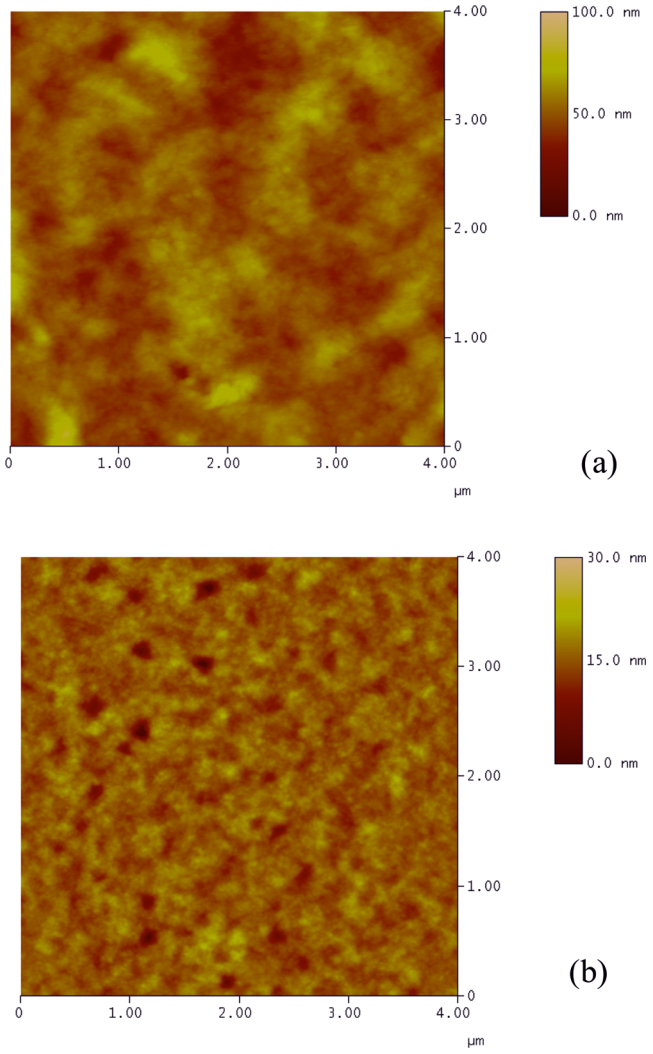

Figure 10. AFM images of (a) P3HT and (b) P3HT:GO-PITC 20% thin films.

exciton generation and charge separation, thus leading to reduced efficiencies.

Despite these promising results, the efficiency of the graphene based OPV devices is still low, about 1 order of magnitude smaller than the fullerene-based devices.[43] However, the polymer-fullerene OPV devices have been extensively optimized for more than a decade. Moreover, the energy level differences of the donor and acceptor materials of the graphene-based system do not match as well as in the polymer-fullerene case. Therefore, extensive research in the design of new graphene-based materials with tailored bandgap and their corresponding polymer donors is urgently needed.

4. CONCLUSIONS

A novel graphene-based material was synthesized, consisting of GO sheets functionalized with phenyl-isothiocyanate side groups. The resulting GO-PITC, which is soluble in *o*-DCB, was successfully blended with P3HT and used as the photoactive layer in bulk heterojunction organic photovoltaic devices. The device containing 20 wt % GO-PITC blended with P3HT, achieved power conversion efficiency (η) of 1.02%, after postfabrication annealing. All the photovoltaic devices were fabricated in air and the measurements were made in air

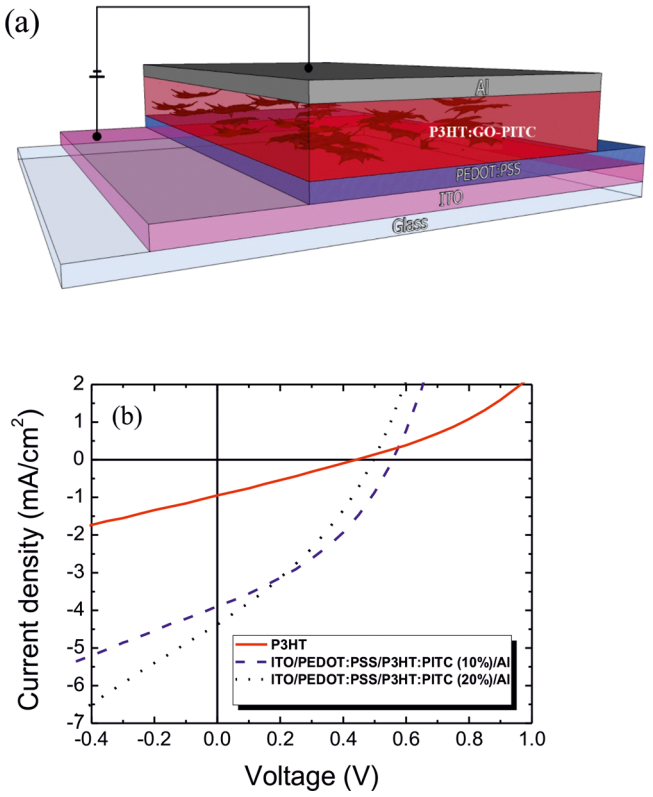

Figure 11. (a) Schematic of the photovoltaic device with P3HT:GO-PITC thin film as the active layer and the structure ITO/PEDOT:PSS(30 nm)/P3HT:GO-PITC(110 nm)/Al(80 nm). (b) Experimental *J*−*V* curves of the photovoltaic devices based on P3HT (red curve) and P3HT:GO-PITC composites (blue curve, 10 wt %; black curve, 20 wt %) after postfabrication thermal annealing at 160 °C for 20 min.

Table 1. Device Performance of Photovoltaic Devices Based on P3HT:GO-PITC Composites with Different GO-PITC Content Following Annealing at 160°C for 20 min

GO-PITC (%)	V_{oc} (V)	J_{sc} (mA/cm^2)	FF (%)	η (%)
0	0.40	0.04	0.28	0.004
10	0.57	3.96	0.39	0.88
20	0.51	4.34	0.46	1.02

immediately after device fabrication. The sufficient photovoltaic performance of GO-PITC, without any optimization, renders this novel graphene-based material as an alternative electron acceptor for OPVs devices. It can be easily anticipated that its performance would be rather enhanced following the proper optimization.

AUTHOR INFORMATION

Corresponding Author

*Tel: 2810-379895. Fax: +30-2810-379845. E-mail: kymakis@staff.teicrete.gr.

Notes

The authors declare no competing financial interest.

ACKNOWLEDGMENTS

This research has been cofinanced by the European Union (European Social Fund, ESF) and Greek national funds through the Operational Program "Education and Lifelong Learning" of the National Strategic Reference Framework

(NSRF) Research Funding Program: Heracleitus II. Investing in knowledge society through the European Social Fund.

REFERENCES

(1) Borchert, H.; Witt, F.; Chanaewa, A.; Werner, F.; Dorn, J.; Dufaux, T.; Kruszynska, M.; Jandke, A.; Hoeltig, M.; Alfere, T.; Boettcher, J.; Gimmler, C.; Klinke, C.; Burghard, M.; Mews, A.; Weller, H.; Parisi, J. *J. Phys. Chem. C* **2012**, *116*, 412−419.
(2) Li, S.-S.; Tu, K.-H.; Lin, C.-C.; Chen, C.-W.; Chhowalla, M. *ACS Nano* **2010**, *4*, 3169−3174.
(3) Valentini, L.; Cardinali, M.; Bittolo Bon, S.; Bagnis, D.; Verdejo, R.; Lopez-Manchado, M.-A.; Kenny, J. M. *J. Mater. Chem.* **2010**, *20*, 995−1000.
(4) Kymakis, E.; Amaratunga, G. A. *J. Appl. Phys. Lett.* **2002**, *80*, 112−114.
(5) Yip, H.-L.; Jen, A. K.-Y. *Energy Environ. Sci.* **2012**, *5*, 5994−6011.
(6) Kymakis, E.; Servati, P.; Tzanetakis, P.; Koudoumas, E.; Kornilios, N.; Rompogiannakis, I.; Franghiadakis, Y.; Amaratunga, G. A. J. *Nanotechnology* **2007**, *18*, 435702−435707.
(7) Stylianakis, M. M.; Mikroyannidis, J. A.; Kymakis, E. *Sol. Energy Mater. Sol. Cells* **2010**, *94*, 267−274.
(8) Po, R.; Carbonera, C.; Bernardi, A.; Tinti, F.; Camaioni, N. *Sol. Energy Mater. Sol. Cells* **2012**, *100*, 97−114.
(9) Stylianakis, M. M.; Kymakis, E. *Appl. Phys. Lett.* **2012**, *100*, 093301−093305.
(10) Geim, A. K.; Novoselov, K. S. *Nat. Mater.* **2007**, *6*, 183−191.
(11) Geim, A. K. *Science* **2009**, *324*, 1530−1534.
(12) Gomez Navarro, C.; Weitz, R. T.; Bittner, A. M.; Scolari, M.; Mews, A.; Burghard, M.; Kern, K. *Nano Lett.* **2007**, *7*, 3499−3503.
(13) Qi, X. Y.; Pu, K. Y.; Zhou, X. Z.; Li, H.; Liu, B.; Boey, F.; Huang, W.; Zhang, H. *Small* **2010**, *6*, 663−669.
(14) Xu, Y. F.; Liu, Z. B.; Zhang, X. L.; Wang, Y.; Tian, J. G.; Huang, Y.; Ma, Y. F.; Zhang, X. Y.; Chen, Y. S. *Adv. Mater.* **2009**, *21*, 1275−1279.
(15) Dreyer, D. R.; Park, S.; Bielawski, C. W.; Ruoff, R. S. *Chem. Soc. Rev.* **2010**, *39*, 228−240.
(16) Dreyer, D. R.; Jia, H. P.; Bielawski, C. W. *Angew. Chem., Int. Ed.* **2010**, *49*, 6813−6816.
(17) Swager, T. M. *ACS Macro Lett* **2012**, *1*, 3−5.
(18) Khan, U.; O'Neill, A.; Lotya, M.; De, S.; Coleman, J. N. *Small* **2010**, *6*, 864−871.
(19) Lomeda, J.; Doyle, C.; Kosynkin, D.; Hwang, W.; Tour, J. *J. Am. Chem. Soc.* **2008**, *130*, 16201−16206.
(20) Xu, Y. X.; Bai, H.; Lu, G. W.; Li, C.; Shi, G. Q. *J. Am. Chem. Soc.* **2008**, *130*, 5856−5857.
(21) Stylianakis, M. M.; Spyropoulos, G. D.; Stratakis, E.; Kymakis, E. *Carbon* **2012**, DOI: 10.1016/j.carbon.2012.08.001.
(22) Su, Q.; Pang, S.; Alijani, V.; Li, C.; Feng, X.; Mullen, K. *Adv. Mater.* **2009**, *21*, 3191−3195.
(23) Englert, J. M.; Rçhrl, J.; Schmidt, C. D.; Graupner, R.; Hundhausen, M.; Hauke, F.; Hirsch, A. *Adv. Mater.* **2009**, *21*, 4265−4269.
(24) Xu, Y.; Zhao, L.; Bai, H.; Hong, W.; Li, C.; Shi, G. *J. Am. Chem. Soc.* **2009**, *131*, 13490−13497.
(25) Ghosh, A.; Rao, K. V.; George, S. J.; Rao, C. N. R. *Chem.—Eur. J.* **2010**, *16*, 2700−2704.
(26) Hill, C. M.; Zhu, Y.; Pan, S. *ACS Nano* **2011**, *5*, 942−951.
(27) Yu, D.; Yang, Y.; Durstock, M.; Baek, J.-B.; Dai, L. *ACS Nano* **2010**, *4*, 5633−5640.
(28) Liu, Q.; Liu, Z.; Zhang, X.; Yang, L.; Zhang, N.; Pan, G.; Yin, S.; Chen, Y.; Wei, J. *Adv. Funct. Mater.* **2009**, *19*, 894−904.
(29) Huang, X.; Qi, X.; Boey, F.; Zhang, H. *Chem. Soc. Rev.* **2012**, *41*, 666−686.
(30) Yu, D.; Park, K.; Durstock, M.; Dai, L. *J. Phys. Chem. Lett.* **2011**, *2*, 1113−1118.
(31) Eda, G.; Fanchini, G.; Chhowalla, M. *Nat. Nanotechnol.* **2008**, *3*, 270−274.
(32) Sun, S.; Cao, Y.; Feng, J.; Wu, P. J. *Mater. Chem.* **2010**, *20*, 5605−5607.
(33) Luo, Z.; Lu, Y.; Somers, L. A.; Johnson, A. T. C. *J. Am. Chem. Soc.* **2009**, *131*, 898−899.
(34) Khan, U.; O'Neill, A.; Porwal, H.; May, P.; Nawaz, K.; Coleman, J. N. *Carbon* **2012**, *2*, 470−475.
(35) Liu, Z.; Liu, Q.; Huang, Y.; Ma, Y.; Yin, S.; Zhang, X.; Sun, W.; Chen, Y. *Adv. Mater.* **2008**, *20*, 3924−3930.
(36) Günzler, H.; Gremlich, H. U. IR Spectroscopy − An Introduction; Wiley-VCH: Weinheim, Germany, 2002; pp 223−227.
(37) Fang, M.; Wang, K.; Lu, H.; Yang, Y.; Nutt, S. J. *Mater. Chem.* **2009**, *19*, 7098−7105.
(38) Stankovich, S.; Dikin, D. A.; Piner, R. D.; Kohlhaas, K. A.; Kleinhammes, A.; Jia, Y.; Wu, Y.; Nguyen, S. T.; Ruoff, R. S. *Carbon* **2007**, *45*, 1558−1565.
(39) Bourlinos, A. B.; Gournis, D.; Petridis, D.; Szabo, T.; Szeri, A.; Dekany, I. *Langmuir* **2003**, *19*, 6050−6055.
(40) Wang, G. X.; Shen, X. P.; Wang, B.; Yao, J.; Park, J. *Carbon* **2009**, *47*, 1359−1364.
(41) Erb, T; Zhokhavets, U; Gobsch, G; Raleva, S; Stuhn, B; Schilinsky, P; Waldauf, C; Brabec, C. J. *Adv. Funct. Mater.* **2005**, *15*, 1193−1196.
(42) Kymakis, E.; Koudoumas, E.; Franghiadakis, I.; Amaratunga, G. A. J. *J. Phys. D: Appl. Phys.* **2006**, *39*, 1058−1062.
(43) Liang, Y.; Xu, Z.; Xia, J.; Tsai, S.-T.; Wu, Y.; Li, G.; Ray, C.; Yu, L. *Adv. Mater.* **2010**, *22*, 135−138.